Cog5–Cog7 crystal structure reveals interactions essential for the function of a multisubunit tethering complex

Jun Yong Ha[a], Irina D. Pokrovskaya[b], Leslie K. Climer[b], Gregory R. Shimamura[a], Tetyana Kudlyk[b], Philip D. Jeffrey[a], Vladimir V. Lupashin[b,c], and Frederick M. Hughson[a,1]

[a]Department of Molecular Biology, Princeton University, Princeton, NJ 08544; [b]Department of Physiology and Biophysics, University of Arkansas for Medical Sciences, Little Rock, AR 72205; and [c]Biological Institute, Tomsk State University, Tomsk, 634050, Russian Federation

Edited by Thomas C. Südhof, Stanford University School of Medicine, Stanford, CA, and approved September 30, 2014 (received for review August 4, 2014)

The conserved oligomeric Golgi (COG) complex is required, along with SNARE and Sec1/Munc18 (SM) proteins, for vesicle docking and fusion at the Golgi. COG, like other multisubunit tethering complexes (MTCs), is thought to function as a scaffold and/or chaperone to direct the assembly of productive SNARE complexes at the sites of membrane fusion. Reflecting this essential role, mutations in the COG complex can cause congenital disorders of glycosylation. A deeper understanding of COG function and dysfunction will likely depend on elucidating its molecular structure. Despite some progress toward this goal, including EM studies of COG lobe A (subunits 1–4) and higher-resolution structures of portions of Cog2 and Cog4, the structures of COG's eight subunits and the principles governing their assembly are mostly unknown. Here, we report the crystal structure of a complex between two lobe B subunits, Cog5 and Cog7. The structure reveals that Cog5 is a member of the complexes associated with tethering containing helical rods (CATCHR) fold family, with homology to subunits of other MTCs including the Dsl1, exocyst, and Golgi-associated retrograde protein (GARP) complexes. The Cog5–Cog7 interaction is analyzed in relation to the Dsl1 complex, the only other CATCHR-family MTC for which subunit interactions have been characterized in detail. Biochemical and functional studies validate the physiological relevance of the observed Cog5–Cog7 interface, indicate that it is conserved from yeast to humans, and demonstrate that its disruption in human cells causes defects in trafficking and glycosylation.

vesicle fusion | COG complex | CATCHR | Golgi | congenital glycosylation disorder

In eukaryotes, the transport of proteins and lipids among intracellular compartments is mediated by vesicular and tubular carriers under the direction of an elaborate protein machinery (1). Among the most complex and least well-characterized components of this machinery are the multisubunit tethering complexes (MTCs) (2). MTCs are thought to mediate the initial attachment (or tethering) between a trafficking vesicle and its target membrane through a constellation of interactions (3, 4). These may include binding of the MTC to activated Rab GTPases, coiled-coil proteins such as Golgins, vesicle coat proteins, SNAREs, Sec1/Munc18 (SM) proteins, and/or membrane lipids. Elucidating the 3D structures of MTCs represents an important step toward a better understanding of their molecular functions.

Four of the known MTCs—termed complexes associated with tethering containing helical rods (CATCHR) or quatrefoil complexes (2, 5)—contain subunits whose shared 3D structure implies a single evolutionary progenitor (6–16). These CATCHR-family MTCs include the Dsl1, Golgi-associated retrograde protein (GARP), exocyst, and conserved oligomeric Golgi (COG) complexes, and they contain three, four, eight, and eight subunits, respectively. Although X-ray or NMR structures have been reported for 14 of these 23 subunits, only one of the structures contains the full-length polypeptide (14). Perhaps more critically, only two subunit interactions—both within the three-subunit Dsl1 complex—have been structurally characterized to date (11, 14). Defining the quaternary structure of the other CATCHR-family MTCs remains a major challenge.

The COG complex is an MTC that is essential for vesicle transport within the Golgi apparatus and from endosomal compartments to the Golgi (3). Defects in individual COG subunits can lead to the aberrant distribution of glycosylation enzymes within the Golgi and thereby to severe genetic diseases known as congenital disorders of glycosylation (CDGs) (17, 18). The first CDG to be attributed to a COG complex defect was traced to a mutation in the *COG7* gene, with infants homozygous for the mutation dying a few weeks after birth (19). Subsequent studies revealed that mutations in most other COG subunits can also give rise to congenital glycosylation disorders (17).

Architecturally, the eight subunits that make up the COG complex can be divided into two subassemblies, lobe A (Cog1, Cog2, Cog3, and Cog4) and lobe B (Cog5, Cog6, Cog7, and Cog8) (20). Single-particle EM of lobe A revealed Y-shaped objects with three long, spindly legs (21). (Thus, the term "lobe"—defined as a roundish and flattish part of something—is a misnomer, at least with respect to Cog1–4.) Partial structures of Cog2 and Cog4 have been reported (6, 12), but the structure of the remainder of the complex, and the nature of the interactions among its subunits, are unknown.

To initiate high-resolution studies of subunit interactions within the COG complex, we began with Cog5 and Cog7. This choice was guided by the observation that recombinant *Saccharomyces*

Significance

In all eukaryotes, the docking and fusion of the vesicles that mediate intracellular trafficking requires multisubunit tethering complexes (MTCs). MTCs are thought to mediate the initial interaction between the vesicle and its target membrane and to orchestrate the assembly of the protein fusion machinery. The largest family of MTCs—of which the conserved oligomeric Golgi (COG) complex is a well-studied member—has been recalcitrant to structural characterization, presumably owing to the size and intrinsic flexibility of the complexes and their constituent subunits. Here we report the initial characterization of subunit interactions within the COG complex by X-ray crystallography. Mutations in the conserved intersubunit interface may be responsible for human congenital glycosylation disorders.

Author contributions: J.Y.H., I.D.P., L.K.C., G.R.S., T.K., P.D.J., V.V.L., and F.M.H. designed research; J.Y.H., I.D.P., L.K.C., G.R.S., T.K., and P.D.J. performed research; J.Y.H., I.D.P., L.K.C., G.R.S., T.K., P.D.J., V.V.L., and F.M.H. analyzed data; and J.Y.H. and F.M.H. wrote the paper.

The authors declare no conflict of interest.

This article is a PNAS Direct Submission.

Data deposition: The atomic coordinates and structure factors have been deposited in the Protein Data Bank, www.pdb.org (PDB ID 4U6U).

[1]To whom correspondence should be addressed. Email: hughson@princeton.edu.

This article contains supporting information online at www.pnas.org/lookup/suppl/doi:10.1073/pnas.1414829111/-/DCSupplemental.

cerevisiae Cog5 and Cog7 form an especially stable binary complex (22). Similarly, comprehensive in vitro cotranslation/coimmunoprecipitation experiments revealed that, among the eight human COG subunits, COG5 and COG7 were unusual in their ability to form a stable binary complex (23). We report here the X-ray structure of a complex containing Cog5 and Cog7 from the yeast *Kluyveromyces lactis.* Our structure reveals Cog5 as an example of the CATCHR fold and elucidates the nature of its interaction with Cog7. We find that the Cog5–Cog7 interface is conserved from yeast to humans and that its disruption causes glycosylation defects in human tissue culture cells and, probably, in a previously identified COG5-CDG patient (24, 25).

Results

X-Ray Structure of a Cog5–Cog7 Complex. Full-length *K. lactis* Cog5 and Cog7 proteins, coexpressed in bacteria, formed a stable, monodisperse complex that was screened for crystallization by using commercially available kits. We obtained crystals under a single condition; these crystals could not, however, be reproduced by using homemade solutions or the same solution from a newer kit. Further investigation revealed that both Cog5 and Cog7 had been cleaved in situ (Fig. S1*A*). The responsible protease was not identified, but it is plausible that it was secreted by a fungal contaminant inadvertently introduced into the commercial screening solution (26). The proteolytic fragments were identified by MS and N-terminal sequencing as Cog5 residues 99–390 and Cog7 residues 81–250. The same fragments could be produced by limited digestion of the original complex with chymotrypsin or proteinase K (Fig. S1*B*). Size-exclusion chromatography of the chymotrypsin digest revealed that $Cog5_{99–390}$ and $Cog7_{81–250}$ eluted at different volumes, inconsistent with their forming a stable complex. Instead, $Cog5_{99–390}$ coeluted with a smaller polypeptide consistent in apparent molecular weight with the remaining N-terminal portion (residues 1–80) of Cog7. Indeed, bacterial coexpression of $Cog5_{99–390}$ and $Cog7_{1–80}$ yielded a stable complex that crystallized reliably.

$Cog5_{99–390}$–$Cog7_{1–80}$ crystals, like the initial crystals of in situ cleaved protein, only diffracted X-rays to 20-Å resolution. A slightly smaller complex, $Cog5_{99–387}$–$Cog7_{5–80}$, crystallized under a wider range of solution conditions, with the best crystals diffracting X-rays to 9–Å resolution. These crystals were further improved through the use of surface entropy reduction (27); ultimately, the best crystals were obtained by changing seven nonconserved residues (five Glu and two Gln) predicted to be located on flexible loops to Ala (*SI Materials and Methods*). The structure was determined by using multiwavelength anomalous diffraction (MAD). In light of the high degree of redundancy within the native data, we determined the effective resolution based on the $CC_{1/2}$ criterion (28), with the final model refined against data to 3.0-Å resolution (*SI Materials and Methods*, Fig. S2, and Table S1).

The $Cog5_{99–387}$–$Cog7_{5–80}$ complex displays a rod-like structure ~30 Å in diameter and 120 Å in length (Fig. 1*A*). $Cog5_{99–387}$ consists of 14 α-helices. A survey of the Protein Data Bank (PDB) using the Dali server (29) revealed strong structural homology with domains A and B of the exocyst subunit Exo70 (Z = 10.2) and somewhat weaker but significant structural homology with other CATCHR-family MTC subunits, including the exocyst subunits Exo84 and Sec6, the GARP complex subunit Vps54, the Dsl1 complex subunits Tip20 and Dsl1, and Cog4 (Z scores ranged from 4.4 to 7.6). Thus, Cog5 joins the growing list of MTC subunits that display the CATCHR fold and are apparently—despite very low levels of sequence homology—derived from a single evolutionary progenitor (6–16).

The structure of $Cog7_{5–80}$ consists of two short helices, α1′ and α2′, and one long helix, α3′ (the prime symbol is used to distinguish Cog7 from Cog5; Fig. 1). All three $Cog7_{5–80}$ α-helices are involved in the interaction with $Cog5_{99–387}$. Conversely, it is primarily helix α1 of $Cog5_{99–387}$ that interacts with $Cog7_{5–80}$. This

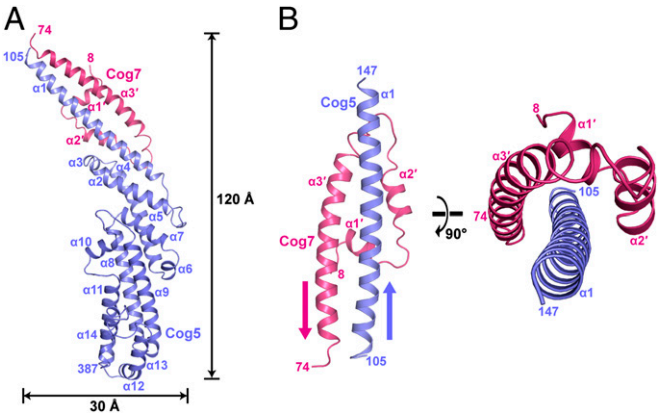

Fig. 1. Overall structure of *K. lactis* Cog5–Cog7 complex. (*A*) Ribbon diagram. (*B*) Close-up highlighting subunit association. Arrows indicate the orientation of Cog5 α1 and Cog7 α3′.

α-helix, Cog5 residues 108–144, represents approximately one quarter of the conserved COG5 domain, residues 11–144, defined by the protein families database Pfam (30). The more N-terminal portions of this conserved region, not present in our structure, could be important for interactions with Cog6, Cog8, and/or COG's functional partners (e.g., Rabs and/or SNAREs).

Previous studies suggest that Cog6 interacts with a Cog5–Cog7 complex to form the structural core of lobe B (22, 23, 31, 32). Consistent with this model, we found that bacterial coexpression of full-length *K. lactis* Cog5, Cog6, and Cog7 yielded a stable, monodisperse complex (Fig. 2*A*). Formation of this complex required only the N-terminal portion of Cog6 (residues 1–209; Fig. 2*B*). Thus, a region representing approximately one quarter of Cog6 was necessary and sufficient for assembly of Cog5–Cog6–Cog7 complexes. Next, we tested whether $Cog6_{1–209}$ was able to bind the truncated Cog5 and Cog7 constructs that had yielded crystals as described earlier. These experiments took advantage of the observation that bacterially expressed $Cog6_{1–209}$ is itself insoluble; therefore, soluble $Cog6_{1–209}$ signifies binding to Cog5 and Cog7. No soluble $Cog6_{1–209}$ was detected when $Cog5_{99–390}$ was substituted for full-length Cog5 or when $Cog7_{5–80}$ was substituted for full-length Cog7 (Fig. S3). Therefore, the N-terminal region of Cog5 and the C-terminal region of Cog7 are required for the formation of a soluble Cog5–$Cog6_{1–209}$–Cog7 complex. The requirement for the N-terminal region of Cog5 is consistent with its conservation as noted earlier.

Structural Basis of the Cog5–Cog7 Interaction. Despite the importance of understanding how CATCHR-family subunits assemble to form MTCs, little relevant structural information has been available. Nonetheless, the interaction between two CATCHR-family subunits in the Dsl1 complex—Tip20 and Dsl1 itself—was inferred from the crystal structure of an artificial Tip20–Dsl1 fusion protein (14). This structure revealed an antiparallel interaction between two α-helices near the N termini of Tip20 and Dsl1 (residues 9–32 and 43–74, respectively; Fig. 3*A*). We discovered by aligning Cog5 and Dsl1 that the interaction between Cog5 α1 and Cog7 α3′ is similar to the inferred interaction between the N-terminal α-helices of Dsl1 and Tip20 (Fig. 3*A*). In particular, the Cog5–Cog7 and the Dsl1–Tip20 interactions entail a coiled-coil interaction between antiparallel α-helices. There are, however, notable differences. The Dsl1 and Tip20 helices are shorter (although this could be explained trivially if the fusion protein lacked sequences needed for the bona fide interaction). A second distinguishing feature of the Cog5–Cog7 interaction is the involvement of the two short Cog7 helices, α1′ and α2′, that, together with α3′, serve to cradle the long Cog5 helix α1 (Figs. 1*B* and 3*A*); Tip20 cannot form helices equivalent to α1′ and

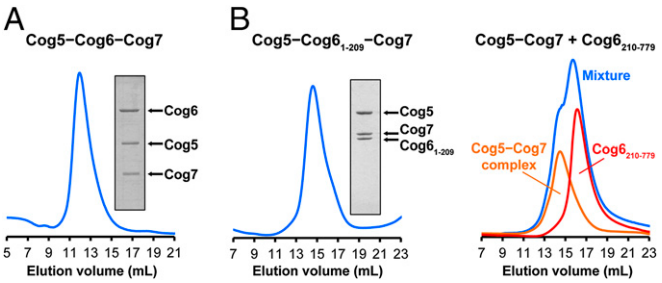

Fig. 2. *K. lactis* Cog6 binds via an N-terminal region to a complex of full-length Cog5 and Cog7. (*A*) Full-length *K. lactis* Cog5, Cog6, and Cog7 form a stable monodisperse complex as judged by size-exclusion chromatography (Superdex 200 10/30). (*B*) An N-terminal region (residues 1–209) of Cog6 is sufficient (*Left*) and necessary (*Right*) for binding to a complex of full-length Cog5 and Cog7.

α2′ because it possesses only nine residues N-terminal to its Dsl1-interacting helix. Overall, the Cog5–Cog7 interaction involves a longer coiled coil, and two additional α-helices, compared with the Dsl1–Tip20 interaction. It is therefore unsurprising that, whereas the Dsl1–Tip20 interaction is rather weak (K_d = 100 μM) (14), Cog5–Cog7 complexes are stable (although the insolubility of uncomplexed Cog5 precludes us from measuring K_d).

The interaction between Cog5 and Cog7 buries 3,010 Å^2 of accessible surface area. Analysis of the Cog5–Cog7 interface reveals key roles for conserved hydrophobic residues. Most of the large Cog5-binding crevice on Cog7 is hydrophobic (Fig. 3*B*). The highly conserved Cog5 residue Leu131 inserts into a hydrophobic pocket formed by largely conserved nonpolar Cog7 residues on helices α2′ and α3′ (Fig. 3 *B* and *C*). The Cog5 residues on either side of Leu131, Leu130 and Arg132, are also highly conserved; Arg132 forms a salt bridge with Asp54′ of Cog7. Together, Cog5 residues Leu130, Leu131, and Arg132 make up an "LLR motif" that appears to be important for binding to Cog7 (as detailed later). Another Cog 5 residue, Ile124, inserts into a second hydrophobic pocket formed by conserved hydrophobic residues on α1′ and α3′ of Cog7. Although there are quite a few potential polar (H-bond and salt bridge) interactions between Cog5 and Cog7, many of them are exposed to solvent and/or involve nonconserved residues, suggesting that van der Waals packing of nonpolar side chains is the salient feature stabilizing the Cog5–Cog7 interface.

To confirm the significance of the crystallographically observed interface, we introduced mutations into full-length GST-Cog5 or full-length His-Cog7 and then tested our ability to recover complexes by using Ni^{2+}-NTA affinity resin. His-Cog7 was recovered in similar yields in all experiments, whereas the recovery of coexpressed GST-Cog5 was dependent on complex formation (Fig. 3*D*). Complex formation was nearly abolished by replacing the central Leu in the Cog5 LLR motif with Asp (L131D). Other single Cog5 mutants, including L130D and R132A as well as I124A, appeared to bind Cog7 normally (Fig. 3*D*). Based on the apparent importance of residue Leu131, we engineered a second set of mutations, this time in Cog7, targeting the residues that contact Leu131 directly: Val27′, Leu31′, Leu50′, and Met53′. Single mutants at three of the four positions disrupted the interaction between GST-Cog5 and His-Cog7 (Fig. 3*D*). Thus, the integrity of the subunit interface observed in the *K. lactis* Cog5$_{99–387}$–Cog7$_{5–80}$ crystal structure is essential for the stability of the complex between full-length Cog5 and full-length Cog7.

Disrupting the COG5–COG7 Interface Impairs COG Function. To test the functional consequences of disrupting the Cog5–Cog7 interaction in vivo, we turned to human cells. Mutations in any of the four human lobe B subunits give rise to CDGs (17). COG5-CDG and COG7-CDG patients display reduced levels of both COG5 and COG7 subunits, consistent with the direct interaction between these subunits (25, 33). We therefore anticipated that disruption of the COG5–COG7 interaction in human cells might have measurable consequences.

First, to confirm that the Cog5–Cog7 interface observed in our *K. lactis* structure is conserved in humans, we used HeLa cells transiently transfected with COG5-3myc and HA-COG7. Binding between COG5-3myc and HA-COG7 was nearly eliminated by changing the central LLR motif residue—Leu176 in human COG5—to Asp (L176D in Fig. 4*A*). Likewise, triple mutants in which Leu176 and its flanking residues (i.e., the entire LLR motif) were modified simultaneously (L175D/L176D/R177E and L175E/L176E/L177E) displayed little or no binding to HA-COG7. The first of these triple mutants, termed COG5(DDE), was used in subsequent experiments described later. We also tested mutations in human COG7. Deleting COG7 residues 2–78, a region corresponding to the *K. lactis* Cog7 fragment (residues 5–80) present in our crystal structure, abolished binding to GFP-COG5; conversely, human COG7 residues 1–156 bound GFP-COG5 efficiently (Fig. 4*B*). Replacing human COG7 residues Ile17′, Phe21′, or Val41′ (corresponding to *K. lactis* Cog7 residues Val27′, Leu31′, or Leu50′) with Asp, singly or in combination, compromised binding (Fig. 4*C*). The triple mutant, termed COG7(DDD), was also used

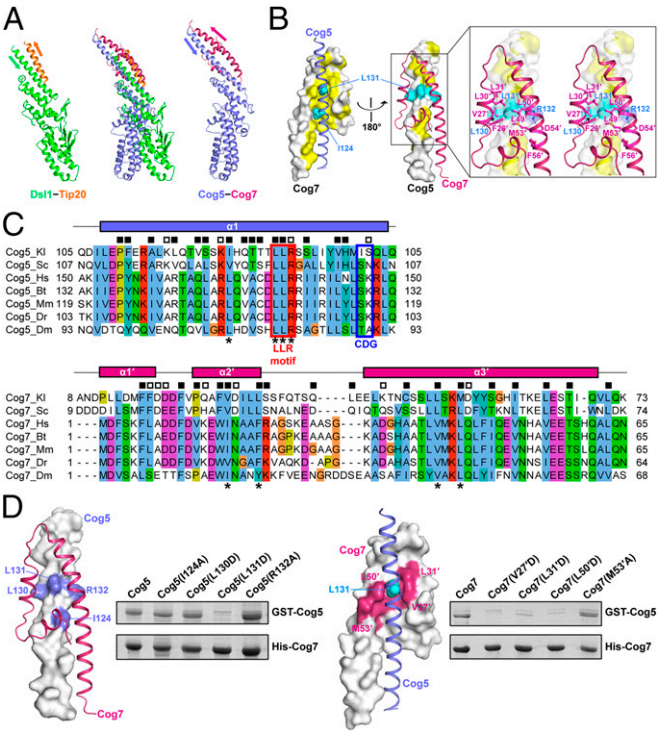

Fig. 3. Interface between *K. lactis* Cog5 and Cog7 and mutations that disrupt it. (*A*) Comparison of Dsl1–Tip20 (PDB ID code 3ETV) and Cog5–Cog7 interfaces. Dsl1 and Cog5 were aligned by using DaliLite (47). (*B*) The Cog5–Cog7 interface. Yellow surface patches represent hydrophobic residues, and cyan surface patch represents the LLR motif. Stereo panels (*Inset*) depict the interactions between the Cog5 LLR motif and Cog7 in detail. (*C*) Sequence alignments of the interacting portions of Cog5 and Cog7. The conserved LLR motif is highlighted, as is the position of the SK→L mutation in the COG5-CDG patient discussed in the text. Intermolecular contacts (using a 4-Å cutoff) are indicated by open (polar) and filled (nonpolar) boxes. Asterisks indicate residues that were mutagenized in *D*. Alignments were calculated by using ClustalW2 (Cog5) and ClustalOmega (Cog7) (48). Bt, *Bos taurus* (F1N1T8); Dm, *Drosophila melanogaster* (Q9VJD3); Dr, *Danio rerio* (F6NMG5); Hs, *Homo sapiens* (Q9UP83); Kl, *K. lactis* (SWISS-PROT accession no. Q6CLE2); Mm, *Mus musculus* (Q8C0L8); Sc, *S. cerevisiae* (P53951). (*D*) Mutational analyses of the interaction between bacterially coexpressed full-length *K. lactis* GST-Cog5 and His-Cog7 (see text for details).

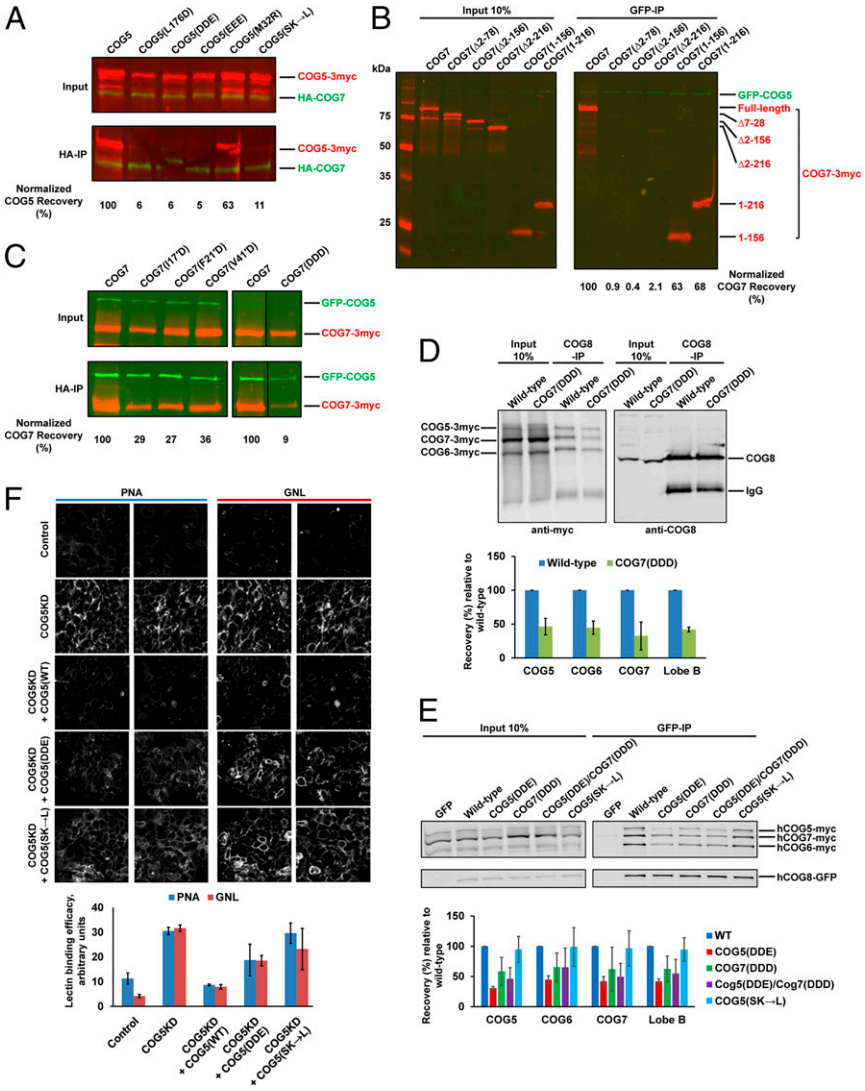

Fig. 4. Functional analyses of the human COG5–COG7 interaction. (*A–C*) Coimmunoprecipitation analysis of the interaction between COG5 and COG7 proteins coexpressed in HeLa cells. (*A*) WT and mutant COG5. (*B*) Full-length COG7 and COG7 fragments. (*C*) WT and mutant COG7. (*D* and *E*) Coimmunoprecipitation analysis of the interaction among lobe B subunits. (*D*) After knocking down endogenous COG5, COG6, and COG7 expression, COG5-3myc, COG6-3myc, and COG7-3myc (WT or DDD) expression plasmids were cotransfected into HeLa cells. One day later, assembled lobe B complexes were recovered from cell lysates using antibodies against endogenous COG8 and analyzed for the presence of COG5-3myc, COG6-3myc, and COG7-3myc (WT or DDD) by Western blotting. The graph depicts the recovery of tagged COG5, COG6, and COG7—and also the average of the three ("Lobe B")—with error bars representing SD between two independent experiments. (*E*) COG8-GFP (or, as a control, GFP) was overexpressed in HEK 293 cells with COG5-3myc (WT, DDE, or SK→L), COG6-3myc, and COG7-3myc (WT or DDD). Assembled lobe B complexes were recovered by using anti-GFP antibodies and analyzed by Western blotting. Error bars indicate SD ($n = 3$). (*F*) PNA and GNL binding to plasma membrane glycoconjugates in control and *COG5* knockdown cells transfected with the indicated expression plasmids. The graph reports the average signal (±SD) in two random fields.

in experiments described later. We note that most mutants were expressed at levels similar to WT, indicating at most a modest effect on stability in vivo. Taken together, our results indicate that the binding interface between *K. lactis* Cog5 and Cog7 is conserved in the corresponding human subunits and that it is essential for the assembly and/or stability of COG5–COG7 complexes.

Previously, we used in vitro cotranslation and coimmunoprecipitation to elucidate the subunit architecture of the human COG complex (23). These experiments revealed that, among all 56 possible pairwise subunit interactions, only four were actually observed: two within lobe A (COG2–COG4 and COG2–COG3), one within lobe B (COG5–COG7), and one linking the two lobes (COG1–COG8). Additional experiments, in which each of the four pairs was combined with each of the six remaining subunits, revealed only two stable three-way interactions: COG2–COG3–COG4 and COG5–COG6–COG7, presumably representing the cores of lobes A and lobe B, respectively. Finally, as expected, COG1–COG2–COG3–COG4 (i.e., lobe A) and COG5–COG6–COG7–COG8 (i.e., lobe B) were observed as four-way interactions. Based on these data, we again turned to transiently transfected human cells to test whether disrupting the COG5–COG7 interaction would destabilize lobe B.

We used two different experiments to test the effect of disrupting the COG5–COG7 interaction on lobe B integrity. In the first, we knocked down expression of COG5, COG6, and COG7 before transfecting HeLa cells with a mixture of plasmids encoding siRNA-resistant COG5-3myc, COG6-3myc, and COG7-3myc. One day later, the cells were lysed and lobe B complexes were immunoprecipitated by using affinity-purified anti-COG8 antibodies. Recovery of COG5, COG6, and COG7 with the endogenous COG8 was reduced approximately twofold in cells expressing, in place of WT COG7-3myc, the COG7(DDD) mutant (Fig. 4*D*). In a second experiment, COG5-3myc, COG6-3myc, COG7-3myc, and COG8-GFP were coexpressed in HEK 293 cells. In these experiments, the tagged subunits are present at approximately fivefold excess over the endogenous subunits. One day later, lobe B complexes were recovered by immunoprecipitation with anti-GFP antibodies. Again, the recovery of intact lobe B complexes was reduced approximately twofold by expressing COG5(DDE), COG7(DDD), or both, in place of the corresponding WT subunits (Fig. 4*E*). The continued recovery of large quantities of intact lobe B demonstrate that neither the COG5(DDE) nor the COG7(DDD) mutations cause global folding defects within their respective subunits. Taken together, these results indicate that disrupting the COG5–COG7 interaction does not dramatically compromise the assembly of lobe B complexes. This may be because COG6 and/or COG8 interact independently with COG5 and COG7, providing a bridging interaction that holds lobe B together in the absence of the COG5–COG7 interaction. Alternatively, COG6 and/or COG8

might stabilize a second interface between COG5 and COG7 that is not contained within our X-ray structure.

COG-mediated vesicle trafficking is required for the proper recycling of glycosyltransferases within the Golgi, defects in which can lead to the aberrant glycosylation of cell surface proteins (34–36). We therefore used lectins—peanut agglutinin (PNA), which recognizes terminal galactosyl residues (37), and *Galanthus nivalis* lectin (GNL), which recognizes terminal mannose residues (38)—to examine the functional consequences of disrupting the interaction between COG5 and COG7. Whereas only low levels of cell surface lectin staining were observed in HEK 293 cells, *COG5* knockdown led to marked increases indicative of aberrant glycosylation (Fig. 4*F*). Aberrant glycosylation in *COG5* knockdown cells was largely rescued by transfection with a plasmid expressing WT COG5-3myc but not by a plasmid expressing COG5(DDE)-3myc (Fig. 4*F*). We conclude that destabilizing the crystallographically observed interaction between COG5 and COG7 disrupts intra-Golgi traffic. That it does so without greatly perturbing the assembly and stability of lobe B (Fig. 4 *D* and *E*) suggests a more direct influence of the COG5–COG7 interface on COG function.

Recently, *COG5* mutations were reported in several CDG patients (24, 25, 39); substantial clinical overlap between COG5-CDG and COG7-CDG was noted (25). Most of the known COG5-CDG patients carry homozygous nonsense or exon skipping mutations (25, 39). Potentially more informative, from a COG structural standpoint, is a patient with relatively mild symptoms and different mutations in her maternal and paternal copies of the *COG5* gene (24, 25). On the maternal allele, two missense mutations replaced Met32 with Arg and Ile619 with Thr (24, 25); neither residue lies within Pfam's conserved COG5 domain. On the paternal allele, a combined deletion/insertion replaced Ser186 and Lys187 with a single Leu (SK→L) (24). Both the deleted residues fall within the conserved COG5 domain; moreover, one of the corresponding *K. lactis* residues (Ser142) contacts Cog7 in our X-ray structure (Fig. 3*C* and Fig. S4). We therefore evaluated the impact of the COG5 deletion/insertion mutation SK→L on COG5–COG7 complex formation. As a control, we also tested the COG5 missense mutation M32R, present on the maternal allele. COG5(SK→L), like COG5 (DDE), displayed a striking defect in COG7 binding (Fig. 4*A*), was successfully incorporated into lobe B complexes (Fig. 4*E*), and failed to rescue the aberrant glycosylation exhibited by COG5 KD cells (Fig. 4*F*). These results strongly suggest that functional deficits caused by disruption of the COG5–COG7 interface can contribute to COG5-CDGs. The relatively mild symptoms exhibited by the patient carrying COG5(SK→L) on the paternal allele can be rationalized by the mitigating effect of the COG5 derived from the maternal allele.

Discussion

We report here what is, to our knowledge, the first structural analysis of lobe B of the COG complex, in which a major portion of the Cog5 subunit was visualized in a complex with an N-terminal fragment of the Cog7 subunit. The X-ray structure revealed that Cog5 adopts a classic α-helical CATCHR fold previously observed in other COG subunits (Cog2, Cog4) and in the Dsl1 (Dsl1, Tip20), exocyst (Sec6, Sec15, Exo70, and Exo84), and GARP (Vps53, Vps54) complexes (6–16). Munc13, a protein implicated in synaptic vesicle docking and fusion, also displays the CATCHR fold (40). Early studies of CATCHR-family MTCs noted that many subunits contain regions predicted to form α-helical coiled coils, suggesting that coiled coil interactions might be responsible for subunit interactions (5, 41–43). The CATCHR fold, however, consists of a series of α-helical bundles difficult to distinguish from coiled coils on the basis of sequence analysis alone. In addition, the predicted coiled coils tend to cluster near the N termini of the subunits, which have been missing from most of the reported structures. The Cog5–Cog7 structure demonstrates that CATCHR-family subunits can, in fact, interact via the formation of an α-helical coiled coil.

A nearly complete model of the Dsl1 complex—at 250 kDa, the smallest MTC of the CATCHR family—was previously assembled from overlapping crystal structures (11, 14). Two of its three subunits display the CATCHR-family fold and were inferred, based on an artificial fusion protein and site-directed mutagenesis, to bind one another by means of an antiparallel interaction between N-terminal α-helices (14). We find here that the interaction between Cog5 and Cog7 is similar and may represent a common subunit interaction mode within the CATCHR-family MTCs. The Cog5–Cog7 interaction can also be viewed in the light of a study of lobe A architecture (21). Single-particle EM of recombinant lobe A containing GFP fiducial markers revealed that the N termini of *S. cerevisiae* Cog1, Cog2, Cog3, and Cog4 intertwine along a proximal segment of one of its three legs. Although high-resolution structural information is not available, the EM data are consistent with a speculative model in which N-terminal α-helices of Cog1 and Cog2 (oriented in one direction) combine with N-terminal α-helices of Cog3 and Cog4 (oriented in the other direction) to form a coiled-coil bundle (21).

Structure-based mutagenesis indicated that the Cog5–Cog7 interaction, centered around the highly conserved LLR sequence motif of Cog5, is conserved from yeast to humans. Unexpectedly, we found that disrupting the human COG5–COG7 interface did not catastrophically disrupt lobe B, which must therefore be stabilized by additional interactions requiring COG6 and/or COG8. Nonetheless, disrupting the COG5–COG7 interface caused aberrant cell surface glycosylation consistent with major deficits in the trafficking of Golgi glycosyltransferases. Although we cannot rule out that a small reduction in the level of lobe B complexes has unexpectedly dire consequences, our results most likely indicate that disrupting the COG5–COG7 interface causes a perturbation in lobe B structure that compromises COG complex function. This conclusion is strengthened by the finding that a COG5-CDG allele [SK→L (24)] maps to the COG5–COG7 interface, destabilizes the binary complex and—without compromising the assembly of lobe B complexes—causes aberrant cell surface glycosylation.

Thus, we find that disrupting the Cog5–Cog7 subunit interaction by directed mutation or in a patient with a congenital glycosylation disorder causes a drastic loss of COG function. That this loss of function is not accompanied by wholesale destabilization of the COG complex suggests that the region around the subunit interaction is specifically required for COG activity. This region might, for example, interact directly with SNARE or SM proteins. It is intriguing in this regard that the region of lobe A where its four subunits interact has been shown to bind the SNARE protein Syntaxin-5 and the SM protein Sly1 (21, 44, 45). SNARE proteins assemble by forming membrane-bridging α-helical coiled-coil bundles, whereas SM proteins interact with and/or modulate formation of these bundles (46). An ability to enter into and/or influence the assembly of α-helical coiled coil bundles might therefore be a common feature uniting CATCHR subunit interfaces with other elements of the trafficking machinery including SNAREs and SM proteins.

In conclusion, we present here initial structural characterization of lobe B of the COG complex, including what is, to our knowledge, the strongest evidence to date that CATCHR subunit interactions are mediated by coiled-coil interactions. Surprisingly, this interaction is not essential for the overall stability of lobe B, but its disruption nevertheless causes severe defects in cell surface glycosylation. It will be important in future work to complete the structure of lobe B, to investigate its mode of interaction with lobe A, and to elucidate the bases for its interactions with functionally significant partners in vesicle docking and fusion.

Materials and Methods

Protein Preparation, Crystallization, and Data Collection. Proteins were overproduced in bacteria and purified by affinity, anion-exchange, and size-exclusion

chromatography. Crystals of native and selenomethionine-substituted *K. lactis* $Cog5_{99–387}$–$Cog7_{5–80}$ complexes were obtained by vapor diffusion at 4 °C after mixing equal volumes of protein (10 mg/mL in 20 mM Tris, pH 8.0, 150 mM NaCl, 2 mM DTT) and well buffer [50 mM Tris, pH 7.5, 2% (wt/vol) PEG 4,000]. As noted earlier, the best crystals were produced by complexes containing $Cog5_{99–387}$ with seven Ala substitutions. Further details are provided in the *SI Materials and Methods*.

Structure Determination and Refinement. The *K. lactis* $Cog5_{99–387}$–$Cog7_{5–80}$ structure was determined via MAD phasing (Table S1); the final refined model includes residues 105–387 of Cog5 and residues 8–74 of Cog7. Details are provided in *SI Materials and Methods*.

Other Methods. Binding experiments and the functional analysis of glycosylation defects are described in *SI Materials and Methods*.

ACKNOWLEDGMENTS. We thank the staff of National Synchrotron Light Source beamlines X25 and X29 for assistance with data collection, Yoshio Misumi for reagents, and Jaak Jaeken and members of our laboratories for discussion. This work was supported by NIH Grants R01 GM071574 (to F.M.H.) and R01 GM083144 (to V.V.L.).

1. Cai H, Reinisch K, Ferro-Novick S (2007) Coats, tethers, Rabs, and SNAREs work together to mediate the intracellular destination of a transport vesicle. *Dev Cell* 12(5): 671–682.
2. Yu IM, Hughson FM (2010) Tethering factors as organizers of intracellular vesicular traffic. *Annu Rev Cell Dev Biol* 26:137–156.
3. Willett R, Ungar D, Lupashin V (2013) The Golgi puppet master: COG complex at center stage of membrane trafficking interactions. *Histochem Cell Biol* 140(3):271–283.
4. Hong W, Lev S (2014) Tethering the assembly of SNARE complexes. *Trends Cell Biol* 24(1):35–43.
5. Whyte JR, Munro S (2002) Vesicle tethering complexes in membrane traffic. *J Cell Sci* 115(Pt 13):2627–2637.
6. Cavanaugh LF, et al. (2007) Structural analysis of conserved oligomeric Golgi complex subunit 2. *J Biol Chem* 282(32):23418–23426.
7. Dong G, Hutagalung AH, Fu C, Novick P, Reinisch KM (2005) The structures of exocyst subunit Exo70p and the Exo84p C-terminal domains reveal a common motif. *Nat Struct Mol Biol* 12(12):1094–1100.
8. Hamburger ZA, Hamburger AE, West AP, Jr, Weis WI (2006) Crystal structure of the *S. cerevisiae* exocyst component Exo70p. *J Mol Biol* 356(1):9–21.
9. Moore BA, Robinson HH, Xu Z (2007) The crystal structure of mouse Exo70 reveals unique features of the mammalian exocyst. *J Mol Biol* 371(2):410–421.
10. Pérez-Victoria FJ, et al. (2010) Structural basis for the wobbler mouse neurodegenerative disorder caused by mutation in the Vps54 subunit of the GARP complex. *Proc Natl Acad Sci USA* 107(29):12860–12865.
11. Ren Y, et al. (2009) A structure-based mechanism for vesicle capture by the multisubunit tethering complex Dsl1. *Cell* 139(6):1119–1129.
12. Richardson BC, et al. (2009) Structural basis for a human glycosylation disorder caused by mutation of the COG4 gene. *Proc Natl Acad Sci USA* 106(32):13329–13334.
13. Sivaram MV, Furgason ML, Brewer DN, Munson M (2006) The structure of the exocyst subunit Sec6p defines a conserved architecture with diverse roles. *Nat Struct Mol Biol* 13(6):555–556.
14. Tripathi A, Ren Y, Jeffrey PD, Hughson FM (2009) Structural characterization of Tip20p and Dsl1p, subunits of the Dsl1p vesicle tethering complex. *Nat Struct Mol Biol* 16(2):114–123.
15. Vasan N, Hutagalung A, Novick P, Reinisch KM (2010) Structure of a C-terminal fragment of its Vps53 subunit suggests similarity of Golgi-associated retrograde protein (GARP) complex to a family of tethering complexes. *Proc Natl Acad Sci USA* 107(32):14176–14181.
16. Wu S, Mehta SQ, Pichaud F, Bellen HJ, Quiocho FA (2005) Sec15 interacts with Rab11 via a novel domain and affects Rab11 localization in vivo. *Nat Struct Mol Biol* 12(10): 879–885.
17. Miller VJ, Ungar D (2012) Re'COG'nition at the Golgi. *Traffic* 13(7):891–897.
18. Freeze HH, Ng BG (2011) Golgi glycosylation and human inherited diseases. *Cold Spring Harb Perspect Biol* 3(9):a005371.
19. Wu X, et al. (2004) Mutation of the COG complex subunit gene COG7 causes a lethal congenital disorder. *Nat Med* 10(5):518–523.
20. Ungar D, et al. (2002) Characterization of a mammalian Golgi-localized protein complex, COG, that is required for normal Golgi morphology and function. *J Cell Biol* 157(3): 405–415.
21. Lees JA, Yip CK, Walz T, Hughson FM (2010) Molecular organization of the COG vesicle tethering complex. *Nat Struct Mol Biol* 17(11):1292–1297.
22. Fotso P, Koryakina Y, Pavliv O, Tsiomenko AB, Lupashin VV (2005) Cog1p plays a central role in the organization of the yeast conserved oligomeric Golgi complex. *J Biol Chem* 280(30):27613–27623.
23. Ungar D, Oka T, Vasile E, Krieger M, Hughson FM (2005) Subunit architecture of the conserved oligomeric Golgi complex. *J Biol Chem* 280(38):32729–32735.
24. Fung CW, et al. (2012) COG5-CDG with a mild neurohepatic presentation. *JIMD Rep* 3:67–70.
25. Rymen D, et al. (2012) COG5-CDG: Expanding the clinical spectrum. *Orphanet J Rare Dis* 7:94.
26. Mandel CR, Gebauer D, Zhang H, Tong L (2006) A serendipitous discovery that in situ proteolysis is essential for the crystallization of yeast CPSF-100 (Ydh1p). *Acta Crystallogr Sect F Struct Biol Cryst Commun* 62(pt 10):1041–1045.
27. Goldschmidt L, Cooper DR, Derewenda ZS, Eisenberg D (2007) Toward rational protein crystallization: A Web server for the design of crystallizable protein variants. *Protein Sci* 16(8):1569–1576.
28. Karplus PA, Diederichs K (2012) Linking crystallographic model and data quality. *Science* 336(6084):1030–1033.
29. Holm L & Rosenstrom P (2010) Dali server: Conservation mapping in 3D. *Nucleic Acids Res* 38(web server issue):W545–549.
30. Finn RD, et al. (2014) Pfam: The protein families database. *Nucleic Acids Res* 42(Database issue):D222–D230.
31. Oka T, et al. (2005) Genetic analysis of the subunit organization and function of the conserved oligomeric golgi (COG) complex: Studies of COG5- and COG7-deficient mammalian cells. *J Biol Chem* 280(38):32736–32745.
32. Laufman O, Freeze HH, Hong W, Lev S (2013) Deficiency of the Cog8 subunit in normal and CDG-derived cells impairs the assembly of the COG and Golgi SNARE complexes. *Traffic* 14(10):1065–1077.
33. Ng BG, et al. (2007) Molecular and clinical characterization of a Moroccan Cog7 deficient patient. *Mol Genet Metab* 91(2):201–204.
34. Shestakova A, Zolov S, Lupashin V (2006) COG complex-mediated recycling of Golgi glycosyltransferases is essential for normal protein glycosylation. *Traffic* 7(2):191–204.
35. Ungar D, Oka T, Krieger M, Hughson FM (2006) Retrograde transport on the COG railway. *Trends Cell Biol* 16(2):113–120.
36. Pokrovskaya ID, et al. (2011) Conserved oligomeric Golgi complex specifically regulates the maintenance of Golgi glycosylation machinery. *Glycobiology* 21(12):1554–1569.
37. Lotan R, Skutelsky E, Danon D, Sharon N (1975) The purification, composition, and specificity of the anti-T lectin from peanut (*Arachis hypogaea*). *J Biol Chem* 250(21): 8518–8523.
38. Van Damme EJM, Allen AK, Peumans WJ (1987) Isolation and characterization of a lectin with exclusive specificity towards mannose from snowdrop (*Galanthus nivalis*) bulbs. *FEBS Lett* 215:140–144.
39. Paesold-Burda P, et al. (2009) Deficiency in COG5 causes a moderate form of congenital disorders of glycosylation. *Hum Mol Genet* 18(22):4350–4356.
40. Li W, et al. (2011) The crystal structure of a Munc13 C-terminal module exhibits a remarkable similarity to vesicle tethering factors. *Structure* 19(10):1443–1455.
41. Kee Y, et al. (1997) Subunit structure of the mammalian exocyst complex. *Proc Natl Acad Sci USA* 94(26):14438–14443.
42. TerBush DR, Maurice T, Roth D, Novick P (1996) The Exocyst is a multiprotein complex required for exocytosis in *Saccharomyces cerevisiae*. *EMBO J* 15(23):6483–6494.
43. Whyte JR, Munro S (2001) The Sec34/35 Golgi transport complex is related to the exocyst, defining a family of complexes involved in multiple steps of membrane traffic. *Dev Cell* 1(4):527–537.
44. Laufman O, Kedan A, Hong W, Lev S (2009) Direct interaction between the COG complex and the SM protein, Sly1, is required for Golgi SNARE pairing. *EMBO J* 28(14): 2006–2017.
45. Shestakova A, Suvorova E, Pavliv O, Khaidakova G, Lupashin V (2007) Interaction of the conserved oligomeric Golgi complex with t-SNARE Syntaxin5a/Sed5 enhances intra-Golgi SNARE complex stability. *J Cell Biol* 179(6):1179–1192.
46. Südhof TC, Rothman JE (2009) Membrane fusion: Grappling with SNARE and SM proteins. *Science* 323(5913):474–477.
47. Holm L, Park J (2000) DaliLite workbench for protein structure comparison. *Bioinformatics* 16(6):566–567.
48. Goujon M, et al. (2010) A new bioinformatics analysis tools framework at EMBL-EBI. *Nucleic Acids Res* 38(web server issue):W695–699.